Published in final edited form as:
*Proc SPIE*. 2014 March 12; 9036: 90362L–. doi:10.1117/12.2043729.

# Identifying MRI markers to evaluate early treatment related changes post laser ablation for cancer pain management

**Pallavi Tiwari**[a], **Shabbar Danish**[b], and **Anant Madabhushi**[a]

[a]Department of Biomedical Engineering, Case Western Reserve University, Cleveland, OH USA

[b]University of Medicine and Dentistry New Jersey, New Brunswick, USA

## Abstract

Laser interstitial thermal therapy (LITT) has recently emerged as a new treatment modality for cancer pain management that targets the cingulum (pain center in the brain), and has shown promise over radio-frequency (RF) based ablation which is reported to provide temporary relief. One of the major advantages enjoyed by LITT is its compatibility with magnetic resonance imaging (MRI), allowing for high resolution in vivo imaging to be used in LITT procedures. Since laser ablation for pain management is currently exploratory and is only performed at a few centers worldwide, its short-, and long-term effects on the cingulum are currently unknown. Traditionally treatment effects are evaluated by monitoring changes in volume of the ablation zone post-treatment. However, this is sub-optimal since it involves evaluating a single global parameter (volume) to detect changes pre-, and post-MRI. Additionally, the qualitative observations of LITT-related changes on multi-parametric MRI (MP-MRI) do not specifically address differentiation between the appearance of treatment related changes (edema, necrosis) from recurrence of the disease (pain recurrence). In this work, we explore the utility of computer extracted texture descriptors on MP-MRI to capture early treatment related changes on a per-voxel basis by extracting quantitative relationships that may allow for an in-depth understanding of tissue response to LITT on MRI, subtle changes that may not be appreciable on original MR intensities. The second objective of this work is to investigate the efficacy of different MRI protocols in accurately capturing treatment related changes within and outside the ablation zone post-LITT. A retrospective cohort of studies comprising pre- and 24-hour post-LITT 3 Tesla T1-weighted (T1w), T2w, T2-GRE, and T2-FLAIR acquisitions was considered. Our scheme involved (1) inter-protocol as well as inter-acquisition affine registration of pre- and post-LITT MRI, (2) quantitation of MRI parameters by correcting for intensity drift in order to examine tissue-specific response, and (3) quantification of MRI maps via texture and intensity features to evaluate changes in MR markers pre- and post-LITT. A total of 78 texture features comprising of non-steerable and steerable gradient and second order statistical features were extracted from pre- and post-LITT MP-MRI on a per-voxel basis. Quantitative, voxel-wise comparison of the changes in MRI texture features between pre-, and post-LITT MRI indicate that (a) steerable and non-steerable gradient texture features were highly sensitive as well as specific in predicting subtle micro-architectural changes within and around the ablation zone pre- and post-LITT, (b) FLAIR was identified as the most sensitive MRI protocol in identifying early treatment changes yielding a

Correspondence to pallavi.tiwari@case.edu.

normalized percentage change of 360% within the ablation zone relative to its pre-LITT value, and (c) GRE was identified as the most sensitive MRI protocol in quantifying changes outside the ablation zone post-LITT. Our preliminary results thus indicate great potential for non-invasive computerized MRI features in determining localized micro-architectural focal treatment related changes post-LITT.

**Keywords**

laser interstitial thermal therapy; cancer pain; focal treatment; treatment change; registration; multi-parametric MRI; monitoring; treatment evaluation

## 1. INTRODUCTION

Nine million people suffer from cancer pain every year with estimated 30% of cancer patients dying with it in the absence of adequate treatment and management.[1] Neuroablative procedures targeting different pain centers have been investigated by neurosurgeons to alleviate the suffering of patients with intractable cancer pain. One such recently investigated procedure is MRI-guided laser interstitial thermal therapy (LITT)[2] that targets the cingulum (pain center in the brain), and may offer measurable advantages for cancer pain management over existing ad-hoc treatment options, such as radio-frequency ablation[3] which only provides temporary pain relief. One of the major advantages enjoyed by LITT is its compatibility with MRI, allowing for high resolution in vivo imaging to be used in LITT procedures. MRI is also capable of monitoring temperature change in the tissue, which enables real-time monitoring of LITT. Further, multi-parametric MRI (MP-MRI) offers the ability to precisely ablate the cingulum via MRI guidance to avoid damage to critical neighboring structures.[2] Although LITT is highly promising for pain management, very little is known about specific early treatment changes caused due to thermal ablation or indeed the accuracy of this procedure in targeting the cingulum and the impact to surrounding tissues.[4]

Given how new LITT technology is for treatment of chronic cancer pain, currently there does not exist any work on evaluating effects of LITT on the cingulum for pain management. However, in the context of evaluating LITT for other neurological applications such as GBM and epilepsy, patients are monitored qualitatively via volumetric analysis on T1-w MRI protocol.[5] T1-w MRI allows for capture of volume of enhancement within ablation focus post-treatment, acquired at regular time intervals (24-hours, 1-month, 3-months, 6-months post-treatment) and comparing these changes with reference to pre-treatment T1-w MRI to identify patients who may still be prone to treatment failure.[5] The volumetric analysis (known as MacDonald criterion[6]) however may be sub-optimal in precisely localizing specific LITT related changes on MRI since it involves evaluating a single parameter (volume) to detect changes pre-, and post-MRI. Additionally, the qualitative observations of LITT-related changes on MP-MRI do not specifically address differentiation between the appearance of treatment related changes (edema, necrosis) from recurrence of the disease (pain recurrence) because of their similar appearance on MRI. The availability of MP-MRI protocols acquired post-LITT provides us with a unique opportunity

to evaluate and monitor localized per-voxel changes across different MRI protocols post-LITT with respect to pre-LITT MRI, and identify MRI markers that correspond to early treatment related changes (such as swelling, edema, and irreversible tissue damage). These early changes are reported to occur as an effect of LITT but have not been studied in the context of pain management.[7,8] A clear understanding of quantitative changes in MR imaging markers corresponding to these treatment changes can serve as a surrogate of treatment response for identification of patients with complete pain relief as against patients with partial or no pain relief. A regular monitoring of MP-MRI markers may also provide us with additional insights on subtle changes in imaging markers that occur within the first few weeks due to the immediate effects of treatment and their role in predicting treatment success. There is hence a significant need for a quantitative approach that allows for evaluation and monitoring of voxel-level changes in imaging markers over time across MP-MRI, and identify sensitive MRI markers that correspond to treatment changes post-LITT.[4] Over the last two decades, texture descriptors have shown tremendous utility in quantifying morphological information for computer aided analysis for a myriad of diseases and tumor types.[9–11] In this work, we explore the applicability of texture descriptors in evaluating early treatment response of LITT towards addressing the following questions in the context of pain-management:

1. Can texture descriptors with MP-MRI quantify early treatment related changes on cingulum for cancer pain-management that may not be appreciable via McDonald criteria or visual inspection of original MRI?
2. Can we identify which MRI marker is more accurate in discerning early treatment related changes within and outside the ablation zone post-LITT? Ideally, MP-MRI parameter should demonstrate large change within the ablation zone and small change within the normal region, as a result of treatment.

Towards addressing these objectives, we present a quantitative approach (Figure 1) for high-resolution (per-voxel) evaluation of early treatment-related changes *in vivo* on MP-MRI, via (a) accurate alignment of different MRI protocols pre- and post-LITT for a per-voxel quantification across different protocols, (b) alignment of intensities via intensity standardization to enable quantitative evaluation of MR parameters across pre- and post-LITT acquisition, while ensuring tissue specific meaning to the parameters being compared, and (c) identification of computer extracted texture descriptors that may better capture early morphological, and micro-architectural changes post-LITT to quantify early treatment related changes post-LITT.

The remainder of the paper is organized as follows. Section 2 discusses the previous work and novel contributions. In Section 3, we provide methodological details of this work. Experimental results are presented in Section 4. We provide concluding remarks in Section 5.

## 2. PREVIOUS WORK AND NOVEL CONTRIBUTIONS

Effects of cingulatomy via radio frequency (RF) treatment (state-of-the-art) on cingulum have been studied in the context of pain-management and depression disorders.[3,12] Yen et

al.[12] evaluated a total of 15 patients who were followed over time to identify signs of pain recurrence or no relief in patients who underwent RF-guided cingulatomy for pain management. Evaluation of patient's response to treatment was performed at regular intervals (1-week, 3-months, and 6-months, and 1-year post treatment). At the end point of evaluation (last available follow up), nine patients had pain relief of more than 50%, six had pain relief between 25 to 50%, and seven had pain improvement of less than 25%. Similarly in Steele et al.,[3] T2-weighted MRI was used to evaluate the best location and volume of the lesions that are associated with a better clinical response for depression patients who underwent RF-cingulatomy. The results suggested that patients when evaluated at 12-month follow-up had a superior clinical response associated with more anterior lesions with small volumes. The authors reported the best clinical response for patients with lesion volume of 1000 to 2000 $cm^3$.

In the context of evaluating quantitative treatment changes post-treatment for other neurological applications, a recent focus has been on quantitatively monitoring changes in MP-MRI markers at different time-points post-treatment during follow-up with respect to baseline (pre-treatment) MRI. Khayal et al.[13] investigated changes in diffusion parameters at pre-, mid-, and post-radiation therapy (RT) for post-surgical Glioblastoma multiforme (GBM) patients to identify imaging markers that correspond to long-term patient survival. The results suggested that the changes in mid- to post-RT were significantly different between patients who progressed within 6-months versus those who were free of progression for 6-months after initiation of therapy. Similarly Foltz et al.[14] evaluated short-term treatment response by evaluating changes in values of ADC and T2 relaxation every 2 weeks within respect to baseline-MRI, over the course of 8 weeks. The significant findings of the work by Foltz et al. included, (a) identifying MRI marker changes that were better correlated with TRC, and (b) identifying an optimal time-point since initiation of treatment, when recurrent disease resurfaced.

Our group[4,15,16] has leveraged these qualitative characteristics within novel quantitative schemes for pervoxel evaluation and MRI signature construction to differentiate between possible radiation treatment outcomes (success, unsuccessful, recurrence). In our recent work,[17] a fiducial driven based registration scheme was presented to evaluate laser ablation changes for GBM and epilepsy patients. Similarly, Viswanath et al.[16,18] recently presented a quantitative approach via texture descriptors in conjunction with MP-MRI to evaluate post-LITT changes for prostate cancer. Texture descriptors were shown to outperform original MR intensities in identifying changes within the ablation zone, pre and post-LITT. Litjens et al.,[19] similarly presented a quantitative approach to distinguishing benign confounding treatment changes from residual prostate cancer on MRI following laser ablation.

In this work, we present the first results of utilizing careful co-registration and image analytic tools to enable high-resolution (per-voxel) evaluation of treatment-related changes *in vivo* in patients who have undergone LITT for pain-management, using MP-MRI information. Additionally, we explore the relative importance and utility of different MRI protocols in determining post-LITT effects. The novel contributions of this work include,

- Application of quantitative image analysis to evaluate treatment-related changes *in vivo* after LITT for chronic cancer pain management, using MP-MRI. The closest work involved studying morphometric changes across MRI to measure regional brain volumes before and after anterior cingulotomy.[3]
- Identification of texture descriptors corresponding to early micro-architectural morphological treatment related changes post-LITT, by quantification of relative sensitivity and change observed in different MP-MRI protocols for evaluating LITT-related treatment change *in vivo*.
- Our methodology is intended to provide a deeper understanding of imaging-related changes due to LITT *in vivo*. These findings may later enable early image-guided intervention in cases of unsuccessful or incomplete treatment, as determined by an MRI-based signature of LITT-related changes.

## 3. METHODOLOGY

### 3.1 Notation

We define $\mathscr{C}_{\beta}^{pre} = \left(C, f_{\beta}^{pre}\right)$ as the pre-LITT MR scene, where $\beta = \{T1w, T2w, GRE, FLAIR\}$ corresponds to the different MR protocols, and $f_{\beta}^{pre}(c)$ is the intensity value associated with every voxel $c$ in a 3D grid $C$. $\mathscr{C}_{\beta}^{post}$ are the corresponding post-LITT MR scenes for every $\beta$, $\beta \in \{T2w, T1w, GRE, FLAIR\}$ that have been aligned to $\mathscr{C}_{\beta}^{pre}$. The region annotated as the ablation zone is denoted $A(C)$ while the normal, benign annotation is denoted $N(C)$.

### 3.2 Inter and intra-protocol registration of pre- and post-LITT MRI

A 3D affine transformation with 12 degrees of freedom, encoding rotation, translation, shear, and scale, is implemented via the 3D Slicer software 4.1. (http://www.slicer.org/) to accurately align post-LITT MRI with reference to the pre-LITT T1w MRI volume, $\mathscr{C}_{T1}^{pre}$, which yielded a registered 3D volume, $\mathscr{C}_{\beta}^{post}$, for every $\beta$, $\beta \in \{T1w, T2w, GRE, FLAIR\}$. During registration, the 3D volume is appropriately resampled and interpolated, in order to account for varying voxel sizes and resolutions between different protocols. Note that all MP-MRI acquisitions are aligned to the pre-treatment frame of reference $C_{T1}^{pre}$ to enable quantitative comparisons (Figure 1(b)).

### 3.3 Correction of MR parameter drift

When the image intensity distributions for $\mathscr{C}_{FLAIR}^{pre}$ (red) and $\mathscr{C}_{FLAIR}^{post}$ (black) were plotted together (Figure 1(c)), it was clear they were not in alignment, implying the presence of intensity drift (or non-standardness)[20] between the pre- and post-LITT acquisitions. A similar trend was observed when plotting the distributions for $\mathscr{C}_{T1w}^{pre}$, $\mathscr{C}_{T2w}^{pre}$, $\mathscr{C}_{GRE}^{pre}$ and corresponding post-imaging, implying the presence of drift in intensity values between pre- and post acquisitions.

The Nyul and Udupa algorithm[21] was implemented to automatically identify corresponding landmarks on each of the histograms, and non-linearly map them to one other. The mapping was calculated as a piece-wise linear transform between corresponding intensity ranges on the histograms of the two acquisitions. As a result of intensity standardization, the histograms were aligned (Figures 1(c)) and the MR parameters could be directly compared.

After segmentation of the lesion ROI on $\mathscr{C}_{T1}^{pre}$, $\mathscr{C}_{\beta}^{pre}$ and $\mathscr{C}_{\beta}^{post}$, $\beta \in \{T1, T2, GRE, FLAIR\}$ are quantitated by correcting for intensity drift between acquisitions.[20] Correcting for this artifact hence enables quantitative comparison of the changes in MR parameters between pre- and post-LITT acquisitions, while ensuring tissue specific meaning to the parameters being compared (Figure 1(c)).

### 3.4 Texture feature extraction of MP-MRI

A total of 78 texture features[11] were extracted from each of $\mathscr{C}_{\beta}^{pre}$, $\mathscr{C}_{\beta}^{post}$, $\beta \in \{T1w, T2w, GRE, FLAIR\}$ on a per-voxel basis. These features are obtained by (1) calculating responses to various filter operators, and (2) computing gray level intensity co-occurrence statistics, as follows,

1. 1. *Non-steerable gradient features*: A set of 17 non-steerable gradient features were obtained via convolution with Sobel and Kirsch edge filters and first-order spatial derivative operators from each of $\mathscr{C}_{\beta}^{pre}$, $\mathscr{C}_{\beta}^{post}$. These operators allow for detection of the strength of horizontal, vertical, and diagonal edges within the image using linear kernels.[22]
2. *Steerable gradient features*: Gabor operators comprise the steerable class of gradient calculations which attempt to match localized frequency characteristics.[23] A Gabor filter can be defined as the modulation of a complex sinusoid by a Gaussian function and is controlled by scale ($\lambda$) and orientation ($\theta$) parameters. 48 Gabor features were extracted from each of $\mathscr{C}_{\beta}^{pre}$, and $\mathscr{C}_{\beta}^{post}$, via convolution with distinct Gabor operators obtained by varying each of the associated parameters.
3. *Second order statistical features*: Second order statistical features have been proposed by Haralick[24] and have found wide application in computing features with perceptual meaning for computerized detection systems.[11] These features are based on quantifying the spatial gray-level co-occurrence within local neighborhoods around each pixel in an image, stored in the form of matrices. 13 Haralick features were calculated from each of $\mathscr{C}_{\beta}^{pre}$, and $\mathscr{C}_{\beta}^{post}$, based on statistics derived from the corresponding co-occurrence matrices.

The reader is directed to [11] for a more detailed description of the individual texture features.

Feature extraction results in feature scenes $\mathscr{F}_{\varphi,\beta}^{k} = \left(C, f_{\varphi,\psi}^{k}\right)$, where $f_{\varphi,\beta}^{k}(c)$ is the feature value at location $c \in C$ when feature operator $\phi$ is applied to scene $\mathscr{C}_{\beta}^{k}$, $\kappa \in \{pre, post\}$, $\beta \in \{T1w, T2w, GRE, FLAIR\}$. For ease of notation, the raw intensity values for every $\beta$ were

included in this set of feature scenes, i.e. there are a total of 79 feature scenes corresponding to each of $\mathscr{C}_{\beta}^{pre}$, $\mathscr{C}_{\beta}^{post}$, $\beta \in \{T1w, T2w, GRE, FLAIR\}$.

### 3.5 Quantifying imaging changes due to LITT

For each of $\mathscr{F}_{\varphi,\beta}^{k}$, $\phi \in \{1, \ldots, 79\}$, $\kappa \in \{pre, post\}$, $\beta \in \{T1w, T2w, GRE, FLAIR\}$, the range of values was normalized to have a mean of 0 and a mean absolute deviation of 1. This ensured that the different parameter values were in a comparable range of values when quantifying differences between pre- and post-LITT MP-MRI.

Calculation of difference statistics was limited to voxels within the annotated regions $A(C)$ and $N(C)$. Due to the focal nature of LITT, it may be expected that regions within $A(C)$ will show large differences between pre- and post-LITT MP-MRI parameters i.e. significant change due to treatment, while regions denoted by $N(C)$ show little to no change due to treatment.

The $L_1$ norm difference between a given pre- and post-LITT MP-MRI feature value can be calculated as

$$\delta_{\varphi,\beta(c)} = f_{\varphi,\beta}^{pre}(c) - f_{\varphi,\beta}^{post}(c), \quad (1)$$

for every voxel $c \in C$ (after normalization).

Difference scenes can be visualized within the ROI (ablation zone) by utilizing a colormap, such that blue corresponds to small difference values and red corresponds to areas of high differences. Therefore, regions annotated as $A(C)$ should be highlighted by red in the difference scene colormap, which would correspond to large changes within the ablation zone due to successful ablation of the lesion focus. Along similar lines, regions annotated as $N(C)$ should be highlighted in blue in the difference scene colormap, corresponding to little to no change in a region not targeted by focal laser ablation (Figure 1(e)).

The normalized percentage change each of $\mathscr{F}_{\varphi,\beta}^{post}$ with respect to the corresponding $\mathscr{F}_{\varphi,\beta}^{pre}$, $\phi \in \{1, \ldots, 79\}$, $\beta \in \{T1w, T2w, GRE, FLAIR\}$ was calculated as,

$$\rho_{\varphi,\beta}^{A} = MEDIAN_{c \in A(C)} \frac{\delta_{\varphi,\beta}(c)}{f_{\varphi,\beta}^{pre}(c)}, \quad (2)$$

$$S(\rho_{\varphi,\beta}) = \left(\rho_{\varphi,\beta}^{A}\right)^2 - \left(\rho_{\varphi,\beta}^{N}\right)^2. \quad (3)$$

$\rho_{\varphi,\beta}^{A}$ and $\rho_{\varphi,\beta}^{N}$ quantify the change in MP-MRI parameter $\phi$ within the annotated regions $N(C)$ and $A(C)$, and are implicitly normalized between 0 and 1, where 1 corresponds to a large difference and 0 corresponds to no difference (between the pre- and post-LITT MRI feature). In an ideal scenario, we would expect that $\rho_{\varphi,\beta}^{A}$ will be close to or greater than 1, corresponding to a large change in the MP-MRI feature $\phi$ within the successfully ablated

region (this would be considered a *highly sensitive* response). Similarly, $\rho^{N}_{\varphi,\beta}$ should ideally be close to 0, corresponding to no change in the MP-MRI feature $\phi$ within the normal region that should largely remain unaffected by focal ablation (implying a *highly specific* response).

### 3.6 Identifying the most sensitive and specific texture descriptor in capturing treatment related changes post-LITT

Each MP-MRI feature was then ranked based on maximizing $\rho^{A}_{\varphi,\beta}$ while minimizing $\rho^{N}_{\varphi,\beta}$, $\phi \in \{1, \ldots, 79\}$, $\beta \in \{T1w, T2w, GRE, FLAIR\}$, via the scoring function

$$S(\rho_{\varphi,\beta}) = \left(\rho^{A}_{\varphi,\beta}\right)^2 - \left(\rho^{N}_{\varphi,\beta}\right)^2. \quad (4)$$

A high value for $S(\rho_{\phi,\beta})$ will correspond to a feature that is highly sensitive (i.e. $\rho^{A}_{\varphi,\beta}$ close to 1) as well as highly specific (i.e. $\rho^{N}_{\varphi,\beta}$ close to 0).

## 4. EXPERIMENTAL DESIGN AND RESULTS

### 4.1 Data Description

An FDA-cleared surgical laser ablation system (Visualase Thermal Therapy System; Visualase, Inc., Houston, TX) was employed for the LITT procedure. Two chronic cancer pain patients were monitored post-LITT at 24-hours via MP-MRI (T1-w, T2-w, GRE, FLAIR) as a part of an ongoing study at University of Medicine and Dentistry, New Jersey (UMDNJ), after initial 3-Tesla MP-MRI. The details of the surgical procedure have been previously described.[25] Briefly, the procedure is performed in the following manner. The appropriate entry point and trajectory angle are identified using the Medtronics Stealth S7 (Medtronics, Inc., Minneapolis, MN) using merged MRI and CT images. A stab incision is made at the entry site, followed by the creation of a burr hole using a handheld 3.2 mm twist drill. The Visualase Thermal Therapy System (Visualase, Inc., Houston, TX) bone anchor is placed using the alignment rod and precision aiming device, and then secured to the calvarium. The laser catheter is introduced through the fixed bone anchor. The laser used in the Visualase system is a 15-W, 980-nm diode laser, flexible diffusing tipped fiber optic, and 17-gauge internally cooled catheter. The patient is transferred to the MRI suite for the remainder of the procedure. In the MRI suite, the Visualase hardware system is connected to the MRI scanner, which allows for real-time thermal monitoring. The delivery of a test dose (typically, 3 W, 2030 seconds), gives confirmation of laser placement. Safety margins are planned using the Visualase software such that the surrounding tissues temperatures do not surpass the predetermined limit (508C) and the center of the lesion does not exceed 908C (to avoid steam). In addition, the software allows for target temperature placement in multiple orthogonal planes if necessary based on the lesion location. Laser treatment is then started at the appropriate dose and duration to achieve maximal lesion destruction. During the ablation procedure, the software imports thermal imaging information every 5 seconds, allowing real-time analysis of the ablation process. There were no partial treatments in this series. Most patients were discharged within 2436 hours in the absence of complications or other general medical conditions.

### 4.2 Experiment 1: Evaluating MRI markers in quantifying early LITT-related changes within and outside ablation zone

Figure 2 shows the top two performing features, based on $S(\rho)$ for T2-FLAIR. Note the pronounced microarchitectural changes across the two texture descriptors (Figure 2(b),(c)) as compared to the original FLAIR image (Figure 2(a)). Table 2 summarizes the top three texture descriptors for T1w, T2w, T2-GRE, and T2-FLAIR MRI ranked in descending order, along with the percentage change between pre, post-LITT values within the ablation zone. It can be observed that Gabor responses were primarily ranked highest within each of the multi-parametric MRI feature sets, based on a scoring function that attempted to maximize percentage change within the ablation zone while minimizing change within a normal region (between pre- and post-LITT MRI features). More specifically, Gabor features (at $\Theta$=1.96, $\Lambda$=11.31) were consistently identified as an important feature in evaluating treatment response across each of the different MRI protocols. This implies the presence of distinct micro-architectural orientation and gradient changes occurring specifically within the ablation zone as a result of LITT, possibly due to the presence of necrotic or ablated tissue in this region. However, normal regions show a markedly lower change in these features, likely because they are unaffected by the focal nature of LITT.

### 4.3 Experiment 2: Relative importance of MRI protocols in quantifying LITT changes within and outside ablation zone

Figures 3(a)-(d) show the barplot results of the top performing features in terms of quantifying treatment related changes post-LITT for each of the different MR protocols, T1w, GRE, T2w, and FLAIR respectively. As apparent from Figure 3, T2-FLAIR accentuated changes with a maximal normalized change (350%) within the ablation zone (Table 2), followed by T2w with a maximal normalized change of 140% as compared to pre-LITT imaging, followed by T1w MRI and GRE. T2w and T2-FLAIR (suppresses cerebrospinal fluid (CSF) to improve contrast) sequences are known to accentuate the appearance of edema and assist in distinguishing edema from normal CSF.[26] T2-GRE was found to characterize a maximal normalized change of 79%, and T1w MRI was reported to capture 75% change in texture descriptors post-LITT. This suggests that FLAIR and T2w MRI may be able to better capture subtle early treatment related changes (such as edema and swelling), as compared to T2-GRE and T1w MRI.

It is interesting to note that GRE was identified to be sensitive in identifying treatment related changes within the normal areas (outside the ablation zone). GRE accentuated a change of 20% in the normal area outside the ablation zone, as compared to pre-LITT imaging. GRE protocol is known to be sensitive to micro-hemorrhage (micro-bleeds) in the brain,[27] and we believe is possibly quantifying acute effect of LITT to normal areas immediately after treatment. GRE was followed by T1w, T2-w and FLAIR MRI in capturing treatment related changes outside the ablation zone post-LITT.

## 5. CONCLUDING REMARKS

LITT holds tremendous potential as a minimally invasive treatment modality for pain management. However, a more widespread adoption of this new, exciting technique would

involve rigorous quantitative evaluation of its treatment related effects, which may be reflected via the changes in MR imaging markers post-LITT. Towards this end, we presented a novel approach via computer extracted texture descriptors to evaluate early morphological changes post-LITT for chronic cancer pain patients. The motivation of this work was to identify texture descriptors that can capture subtle micro-architectural changes (caused due to fundamental changes induced by LITT) that may not be discernible on the raw MR intensity images. We believe that a quantitative approach to evaluation of treatment-related changes between pre- and post-LITT MP-MRI may also allow for the building of a novel imaging-based prognostic indicators of patient treatment response. Our framework leveraged registration and feature extraction tools to accurately quantify treatment related changes on a per-voxel basis on different MRI protocols. Our preliminary results based on 2 patient studies indicate that,

- Computerized textural descriptors derived from multi-parametric MRI result in distinctly more sensitive and specific responses, evaluated on a voxel-by-voxel basis, within the ablation zone that were successfully ablated compared to normal regions.
- Gabor features (specifically at orientation, $\Theta$=1.96, and wavelength, $\Lambda$=11.31) are consistently identified as the highest ranked features for accurately quantifying LITT-related changes across all MRI protocols. These texture descriptors visualize responses across multiple scales, directions, and gradients, and are possibly quantifying changes in micro-architectural glandular orientation specifically occurring within the ablation zone, as a result of fundamental changes in tissue architecture induced by LITT.
- FLAIR, T2-w MRI were identify to exaggerated early LITT-effects within ablation zone, while GRE, T1-w MRI protocols exaggerated LITT-effects outside the ablation zone.

Our approach is intended to form a precursor to building of a novel imaging-based predictor of early focal treatment response to enable effective image-guided intervention for pain management. However, in the absence of a larger cohort of data and long-term follow-up MRI information, this work was limited to evaluating early treatment related changes (edema, swelling) post-LITT. Given a larger cohort of data including more follow-up MRI acquisition, the current framework is readily extensible to identify computerized MR markers corresponding to a long-term patient's response to therapy. Additionally, we plan to examine computerized MRI descriptors on follow-up MRI corresponding to delayed treatment related changes, such as thermal necrosis. Our scheme may also find application in examining quantitative changes in non-invasive imaging markers as a function of time, to be correlated against complete pain relief.

## Acknowledgments

Research reported in this publication was supported by the National Cancer Institute of the National Institutes of Health under award numbers R01CA136535-01, R01CA140772-01, and R21CA167811-01; the National Institute of Diabetes and Digestive and Kidney Diseases under award number R01DK098503-02, the DOD Prostate Cancer Synergistic Idea Development Award (PC120857); the QED award from the University City Science Center and Rutgers University, the Ohio Third Frontier Technology development Grant, and the Coulter foundation award. The

content is solely the responsibility of the authors and does not necessarily represent the offi cial views of the National Institutes of Health.

## REFERENCES

[1]. Vuorinen E. Pain as an early symptom in cancer. Clin J Pain. 1993; 9(4):272–278. [PubMed: 8118092]

[2]. Beccaria K, Canney M, Carpentier A. Magnetic resonance-guided laser interstitial thermal therapy for brain tumors. Tumors of the Central Nervous System. 2012; 5(23):173–185.

[3]. Steele J, Christmas D, Eljamel M, Matthews K. Anterior cingulotomy for major depression: Clinical outcome and relationship to lesion characteristics. Biol Psychiatry. 2007; 63(7):670–77. [PubMed: 17916331]

[4]. Tiwari P, Shabbar D, Stephen W, Madabhushi A. Quantitative evaluation of multi-parametric MR imaging marker changes post-LITT for epilepsy. Proc. SPIE. 2013; 8671:1–13.

[5]. Curry D, Gowda A, McNichols R, Wilfong A. MR-guided laser ablation of epileptogenic foci in children. Epilepsy and Behavior. 2012; 24:408–414. [PubMed: 22687387]

[6]. Macdonald D, Cascino T, Schold S, Cairncross J. Response criteria for phase ii studies of malignant glioma. J Clin Oncol. 1990; 8:127780.

[7]. Morrison P, Jolesz F, Charous D, Mulkern, Ran Hushek S, Margolis R, Fried M. MRI of Laser-induced Interstitial Thermal Injury in an *in-vivo* animal liver model with histologic correlation. J Magn Reson Imaging. 1998; 8:57–63. [PubMed: 9500261]

[8]. Mller-Lisse G, Heuck A, Stehling M, Frimberger M, Thoma M, Schneede P, Muschter R, Hofstetter A, Reiser M. Mri monitoring before, during and after interstitial laser-induced hyperthermia of benign prostatic hyperplasia. initial clinical experiences. Radiology. 1996; 36(9): 722–731.

[9]. Moura D, Lpez MG. An evaluation of image descriptors combined with clinical data for breast cancer diagnosis. IJCARS. 2013; 8(4):561–74.

[10]. Nanni L, Brahnam S, Ghidoni S, Menegatti E, Barrier T. Different approaches for extracting information from the co-occurrence matrix. PLOS ONE. 2013; 8(12):e83554. [PubMed: 24386228]

[11]. Viswanath S, Bloch N, Chappelow J, Toth R, Rofsky N, Genega E, Lenkinski R, Madabhushi A. Central gland and peripheral zone prostate tumors have significantly different quantitative imaging signatures on 3 Tesla endorectal, T2-w MR imagery. JMRI. 2012; (1):213–24. [PubMed: 22337003]

[12]. Yen C, Kung S, Su Y, Lin W, Howng S, Kwan A. Stereotactic bilateral anterior cingulotomy for intractable pain. JCN. 2005; 12(8):886–90.

[13]. Khayal I, Polley M, Jalbert L, Elkhaled A, Chang S, Cha S, Butowski N, Nelson S. Evaluation of diffusion parameters as early biomarkers of disease progression in glioblastoma multiforme. Neuro Oncology. 2010; 12(9):908–916. [PubMed: 20501631]

[14]. Foltz W, Wu A, Chung P, Catton C, Bayley A, Milosevic M, Bristow R, Warde P, Simeonov A, Jaffray D, Haider M, Mnard C. Changes in apparent diffusion coe cient and t2 relaxation during radiotherapy for prostate cancer. Journal of Magnetic Resonance Imaging. 2012 [Epub ahead of print].

[15]. Tiwari, P.; Viswanath, S.; Kurhanewicz, J.; Madabhushi, A. Weighted combination of multi-parametric mr imaging markers for evaluating radiation therapy related changes in the prostate. Workshop on Prostate Cancer Imaging (in conjunction with MICCAI); 2011. p. 8091

[16]. Viswanath, A.; Tiwari, P.; Chappelow, J.; Toth, R.; Kurhanewicz, J.; Madabhushi, A. Cadonc: An integrated toolkit for evaluating radiation therapy related changes in the prostate using multiparametric mri. Biomedical Imaging: From Nano to Macro, IEEE International Symposium; 2011. p. 2098

[17]. Wan T, Bloch B, Danish S, Madabhushi A. A learning based fiducial-driven registration scheme for evaluating laser ablation changes in neurological disorders. Neurocomputing. 2014 (pre-print).

[18]. Viswanth S, Toth R, Rusu M, Sperling D, Lepor H, Futterer J, Madabhushi A. Identifying quantitative in vivo multi-parametric mri features for treatment related changes after laser interstitial thermal therapy of prostate cancer. Neurocomputing. 2014 (pre-print).

[19]. Litjens G, Huisman H, Elliott R, Shih N, Feldman M, Viswanath S, Fütterer J, Bomers J, Madabhushi A. Distinguishing benign confounding treatment changes from residual prostate cancer on mri following laser ablation. SPIE. 2014 (pre-print).

[20]. Madabhushi A, Udupa J. New methods of MRI intensity standardization via generalized scale. Med. Phy. 2006:3426–34.

[21]. Nyul L, Udupa J, Zhang X. New variants of a method of mri scale standardization. Medical Imaging, IEEE Transactions. 2000:143150.

[22]. Agner S, Soman S, Libfeld E, McDonald M, Thomas K, Englander S, Rosen M, Chin J, Nosher D, Madabhushi A. Textural kinetics: A novel dynamic contrast-enhanced (dce)-mri feature for breast lesion classification. J Digit Imaging. 2010; 24:44663.

[23]. Wang Y, Chua C. Face recognition from 2d and 3d images using 3d gabor filters. Image and Vision Computing. 2005; 23(11):10181028.

[24]. Haralick R, Shanmugam K, Dinstein I. Textural features for image classification. IEEE Trans Sys Man Cybernetics. 1973; 3(6):610621.

[25]. Jethwa P, Barrese J, Gowda A, Shetty A, Danish S. Magnetic resonance thermometry-guided laser-induced thermal therapy for intracranial neoplasms: Initial experience. Neurosurgery. 2012; 71(1 Suppl Operative):133144.

[26]. Tsuchiya K, Mizutani Y, Hachiya J. Preliminary Evaluation of Fluid-Attenuated Inversion-Recovery MR in the Diagnosis of Intracranial Tumors. AJNR Am J Neuroradiol. 1996:10811086.

[27]. Lin D, Flippi C, Steever A, Zimmerman R. Detection of intracranial hemorrhage: comparison between gradient-echo images and b(0) images obtained from diffusion-weighted echo-planar sequences. AJNR Am J Neuroradiol. 2001; 22(7):1275–81. [PubMed: 11498414]

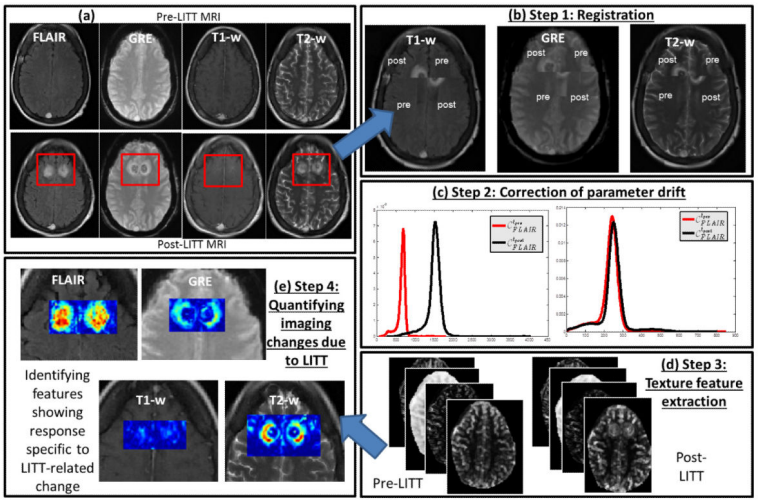


**Figure 1.**
Overview of the methodology and overall workflow.

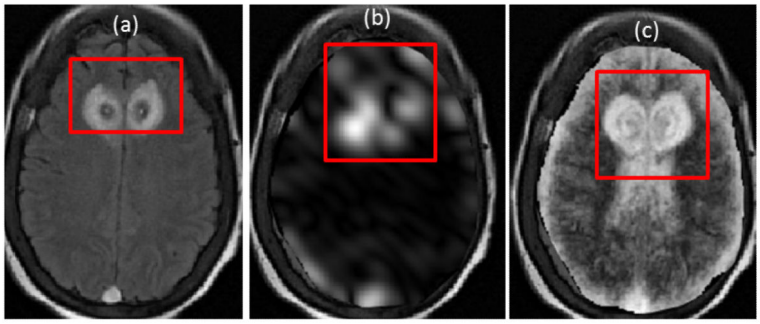


**Figure 2.**

(a) original FLAIR image, (b), (c) show top two texture descriptors identified via $S(\rho_{\phi,\beta})$. Note the exaggerated response of texture descriptors around the ablation zone which is not discernible on (a).

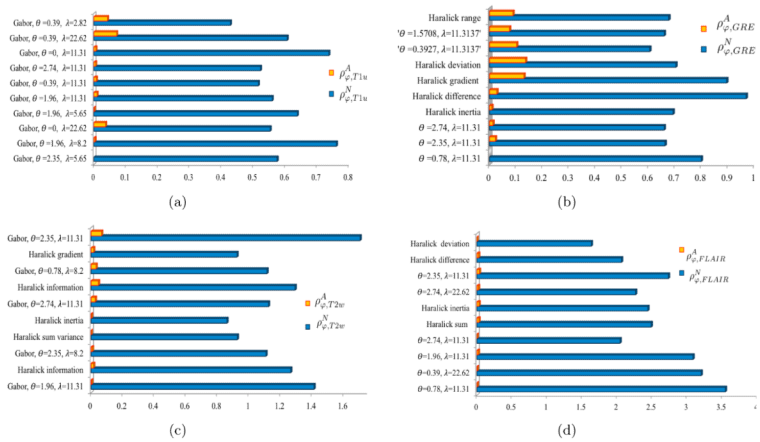


**Figure 3.**

Top 10 features for every MRI protocol, ranked in descending order based on $S(\rho_{\phi,\beta})$, $\beta \in \{T1w, T2w, GRE, FLAIR\}$ i.e. showing a high change within the ablation regions and a low change within normal regions.

**Table 1**

List of texture features employed in this work to evaluate early treatment response post-LITT.

| Modality | Feature set | Significance |
|---|---|---|
| T2-w, T1-w, FLAIR, GRE | Grey-level statistics | Features capturing summary statistics such as mean, standard deviation and derivative features of pixels values within a localized neighborhood. |
| | Gabor wavelet transform | Textural representation obtained via convolution of an image within Gabor filter bank, which comprised filters with different frequencies and orientations. |
| | Haralick Texture | Statistics of gray-level co-occurrence matrices such as angular second moment, contrast and difference entropy |

## Table 2

Top 3 texture descriptors listed for T2-FLAIR, T2w, T2-GRE, and T1w MRI protocols.

| MRI protocol | texture descriptor | $S(\rho_{\phi i})$(%) |
|---|---|---|
| FLAIR | **Gabor**, Θ = 0.78, Λ=**11.31** | 354% |
| | Gabor, Θ = 0.39, Λ=22.62 | 319% |
| | **Gabor**, Θ=**1.96**, Λ=**11.31** | 307% |
| T2w | **Gabor**, Θ=**1.96**, Λ=**11.31** | 141% |
| | Haralick information | 126% |
| | Gabor, Θ = 2.35, Λ=8.2 | 110% |
| GRE | **Gabor**, Θ = 0.78, Λ=**11.31** | 79% |
| | **Gabor**, Θ=**1.96**, Λ=**11.31** | 66% |
| | Gabor, Θ = 2.74, Λ=11.31 | 65% |
| T1 | **Gabor**, Θ=**1.96**, Λ=8.2 | 75% |
| | Gabor, Θ = 2.35, Λ=5.65 | 57% |
| | Gabor, Θ = 0, Λ=22.62 | 55% |